Received: 25 March 2020 | Revised: 6 December 2020 | Accepted: 7 December 2020

DOI: 10.1002/alz.12289

Alzheimer's & Dementia®
THE JOURNAL OF THE ALZHEIMER'S ASSOCIATION

FEATURED ARTICLE

CVN-AD Alzheimer's mice show premature reduction in neurovascular coupling in response to spreading depression and anoxia compared to aged controls

Dennis A. Turner[1,2,3,4] | **Simone Degan**[1,4] | **Ulrike Hoffmann**[5] | **Francesca Galeffi**[1,4] | **Carol A. Colton**[6]

[1] Neurosurgery, Box 3807, Duke University Medical Center, Durham, North Carolina 27710, USA

[2] Neurobiology, Box 3209, Duke University Medical Center, Durham, North Carolina 27710, USA

[3] Biomedical Engineering, Box 90281, Duke University, Durham, North Carolina 27708, USA

[4] Research and Surgery Services, Durham VA Medical Center, 508 Fulton Street, Durham, North Carolina 27705, USA

[5] Anesthesiology, Box 3094, Duke University Medical Center, Durham, North Carolina 27710, USA

[6] Neurology, Box 2900, Duke University Medical Center, Durham, North Carolina 27710, USA

Correspondence
Dennis A. Turner MA, MD, Neurosurgery, Box 3807, DUMC, Duke South Blue Zone, Durham, NC 27710, USA.
E-mail: dennis.turner@duke.edu

Funding information
NIH, Grant/Award Numbers: R21 AG051103, VA I21 RX002223, VA I21 BX003023

[The copyright line for this article was changed on April 16, 2021 after original online publication.]

Abstract

We compared the efficacy of neurovascular coupling and substrate supply in cerebral cortex during severe metabolic challenges in transgenic Alzheimer's [CVN-AD] and control [C57Bl/6] mice, to evaluate the hypothesis that metabolic insufficiency is a critical component of degeneration leading to dementia. We analyzed cerebral blood flow and metabolic responses to spreading depression (induced by K^+ applied to the cortex) and anoxia across aging in CVN-AD + C57Bl/6 genotypes. In the CVN-AD genotype progression to histological and cognitive hallmarks of dementia is a stereotyped function of age. We correlated physiology and imaging of the cortex with the blood flow responses measured with laser doppler probes. The results show that spreading depression resulted in a hyperemic blood flow response that was dramatically reduced (24% in amplitude, 70% in area) in both middle-aged and aged CVN-AD mice compared to C57Bl/6 age-matched controls. However, spreading depression amplitude and conduction velocity (≈6 mm/min) did not differ among groups. Anoxia (100% N_2) showed significantly decreased (by 62%) reactive blood flow and autoregulation in aged AD-CVN mice compared to aged control animals. Significantly reduced neurovascular coupling occurred prematurely with aging in CVN-AD mice. Abbreviated physiological hyperemia and decreased resilience to anoxia may enhance early-onset metabolic deficiency through decreased substrate supply to the brain. Metabolic deficiency may contribute significantly to the degeneration associated with dementia as a function of aging and regions of the brain involved.

1 | NARRATIVE

1.1 | Contextual background and disease implications

Stroke occurrence, abnormal metabolism, and loss of blood vessel regulation in the brain can together lead to neurodegeneration, the underlying mechanism of dementia syndrome.[1] Stroke may be preventable through control of medical risk factors and systemic conditions. However, abnormal metabolism and low glucose uptake are present even early in mild cognitive impairment (MCI), a transition in time and disease progression between normal aging and clear Alzheimer's disease (AD) dementia.[2,3] Brain metabolism interacts with blood vessel regulation through neuronal activity signaling, which

This is an open access article under the terms of the Creative Commons Attribution-NonCommercial-NoDerivs License, which permits use and distribution in any medium, provided the original work is properly cited, the use is non-commercial and no modifications or adaptations are made.
© 2021 The Authors. *Alzheimer's & Dementia* published by Wiley Periodicals LLC on behalf of Alzheimer's Association. This article has been contributed to by US Government employees and their work is in the public domain in the USA

functions to increase brain blood flow to accommodate the brain's need for metabolic supply.[4] This dynamic regulation of blood flow by neuronal activity is called neurovascular coupling, in which neurons, astrocytes, and blood vessels interact to continuously match substrate supply (through blood flow) with ongoing metabolic requirements. In the prolonged transition between aging, MCI, and dementia both neurovascular coupling and blood–brain barrier (BBB) function are progressively perturbed. These changes reduce supply of glucose to the brain, compounding the intrinsic reduction in the brain's ability to metabolize glucose.[5]

Oxygen can diffuse from hemoglobin in blood vessels across the BBB into the brain. In contrast, glucose transport across the BBB must be facilitated by transport (glucose) carriers which are severely constrained in dementia.[6] Blunted neurovascular coupling together with diminished glucose transport can significantly reduce glucose entry into the brain.[7] If brain blood flow and/or glucose transport are truncated then intermittent low glucose conditions can disrupt metabolism in spite of metabolic demand. These conditions may starve neurons and cause heightened neuronal damage and worsening dementia.[8] As predicted from human glucose uptake studies showing that impaired metabolism may occur early in dementia,[2,9,10] metabolic insufficiency in the brain may be present over years, causing progressive degeneration and the severe atrophy and neuronal loss associated with dementia. If inadequate neurovascular coupling early in the disease could be estimated by surrogate biomarkers, such as metabolic brain studies with dynamic activation[11] then these patients may be more amenable to early metabolic treatment paradigms.[2]

Further, calcium levels within cells may rise due to reduced metabolism and insufficient transmembrane transport that are required to maintain normal physiological concentrations. These changes add to the already abnormal neuronal calcium levels that result simply from aging (i.e., the calcium hypothesis; see Alzheimer's Association Calcium Hypothesis Workgroup[12]). Our experimental hypothesis is that reduced brain glucose availability significantly contributes to neurodegeneration through episodes of low glucose and high calcium, arising mainly from insufficient neurovascular coupling. Thus, progressive degeneration results from a critical mismatch of metabolic supply and demand.[13]

Because neurovascular coupling is a dynamic process, measuring baseline blood flow during periods of low metabolism may not reveal true, underlying deficits. Hence, cerebral blood flow and substrate uptake need to be assessed during brain activation conditions in which demand is high, to fully determine whether supply can match this demand. Maximal brain activation occurs with high potassium levels around neurons in the brain[14] and requires significant metabolic support to restore neuronal homeostasis. However, neurovascular coupling abnormalities in mouse models of dementia have primarily been studied with mild dynamic brain activation, which may not show critical deficits—these include carbon dioxide changes (which cause vasodilation but not neuronal activation) and sensory activation.[15,16] In contrast, high potassium levels cause severe neuronal depolarization, which can spread across the brain, termed spreading depression.[14] These spreading depression events do occur in humans but are triggered primarily after stroke and head injury when intrinsic damage to the brain can cause focal areas of high potassium levels.[17]

AD neurovascular, cognitive changes, and progressive dementia are observed in mouse models, but in a compressed time course compared to the human transition between normal aging, MCI, and dementia. These pathological changes in mice occur over a stereotypic time course as a function of mouse age.[18] As in humans, age is a critical risk factor for development of dementia in mouse models, including histological changes (i.e., loss of neurons, development of plaques and tangles), behavioral abnormalities (i.e., memory loss), and BBB changes. Animal age in dementia models commonly translates into severity of degeneration and can be more predictable than in humans.

Research in Context

Systematic Review: The authors reviewed both traditional and referenced sources on cerebral blood flow and neurovascular coupling in mouse Alzheimer's models and aging controls in response to spreading depression and anoxia. Relevant citations are appropriately cited.

Interpretation: Our findings show significantly reduced neurovascular coupling and hyperemia in neocortex at earlier ages in a mouse Alzheimer's model (compared to age-matched controls) that demonstrates pathological changes, including perivascular amyloid accumulation, relevant to the human sporadic disease. This reduction in neurovascular coupling may enhance early-onset metabolic deficiency and thereby contribute to inherent neuropathology.

Future Directions: Future experiments will compare the hippocampus to the neocortex and assess if metabolic deficiency precedes pathological development. Direct recordings of dynamic glucose and oxygen supply to the brain will be measured to analyze metabolic deficiency directly. Further, cellular glucose uptake and metabolism will be assessed in this model, and eventually compared to additional mouse models and the human sporadic disease.

Highlights

1. We assess the metabolic deficiency theory of Alzheimer's disease in CVN-AD cortex.
2. Aging-related changes occur with spreading depression responses in mice.
3. Hemodynamic responses to spreading depression are prematurely reduced in CVN-AD mice.
4. The reactive hyperemic response to anoxia is severely compromised in CVN-AD mice.
5. Decreased neurovascular coupling may contribute to metabolic deficiency in CVN-AD mice.

Animal models also allow targeted experiments where spreading depression events can be induced as a function of age by adding a focal potassium source onto the brain, to more adequately test enhanced blood flow (and indirectly substrate) supply to the brain in response to a severe metabolic demand. By testing these spreading depression events across age, we can compare spontaneous aging neurovascular responses occurring in control animals to responses affected by degeneration in the transgenic animal model with AD-like stigmata.[19] During spreading depression events, there is also significant calcium increase within neurons, which may be intrinsically damaging through loss of control of calcium-mediated signaling. Thus, the neurovascular and metabolic responses to spreading depression events and anoxia can help to understand altered mechanisms of neurovascular coupling in dementia development. Additionally, these metabolic demands stringently test the reserve of the brain's vascular supply under severe metabolic stress, as a function of normal aging and dementia.

To test our novel hypothesis of metabolic supply insufficiency with strong metabolic activation, we compared the efficacy of neurovascular coupling in cerebral cortex in transgenic Alzheimer's (CVN-AD) and control (C57Bl/6) mice.[20] We analyzed cerebral blood flow responses to spreading depression and anoxia across three critical age groups in CVN-AD + C57Bl/6 genotypes in vivo. At the older two age groups, CVN-AD mice typically show progressive degeneration, memory loss, and AD stigmata in the stereotypic evolution in these mice.[18] We found that potassium-induced spreading depression resulted in a blunted hyperemic blood flow response that was significantly reduced (24% in amplitude, 70% in area) in both middle-aged and aged CVN-AD mice compared to C57Bl/6 age-matched controls. Anoxia (100% N2) also showed a dramatic decrease (by 62%) in reactive blood flow and autoregulation in aged AD-CVN mice. Significantly reduced neurovascular coupling occurred prematurely with aging in CVN-AD mice, correlating with onset of degeneration and dementia. Abbreviated physiological hyperemia and decreased resilience to anoxia may enhance early onset metabolic deficiency through decreased substrate supply to the brain, a critical element in neuronal degeneration and dementia.

This process of insufficient neurovascular coupling likely worsens over time in response to the myriad, dynamic metabolic needs of the brain, leading to enhanced degeneration as a function of time and age. In addition to the temporal element of metabolic insufficiency, some regions of the brain are more susceptible to degeneration and ischemia, particularly the hippocampus. Thus, in the CVN-AD transgenic animal model, age correlates tightly with progressive loss of learning and memory (cognitive changes often considered critical aspects of dementia in humans) and neurodegeneration, but is compressed compared to the human condition. Like human dementia syndrome, there is also regional and spatial specificity, with the hippocampus being involved prior to the neocortex.[18] Thus, in addition to studying the neocortex, as we have done here, one next step is continuing an age-related study but across additional brain regions, particularly the hippocampus. In the more vulnerable hippocampus, neuronal degeneration may occur earlier, with abnormal neurovascular coupling also expected to be an element in metabolic insufficiency early in the disease process. Key residual questions include the mechanisms underlying the defective neurovascular coupling, and whether even earlier changes occur in the hippocampus, which shows a more progressive degeneration process than the cortical surface of the brain.

If glucose transport is a critical limitation, this may be upregulated through glucagon-like-peptide (GLP-1) agonists to possibly prevent degeneration if caught early.[21] For example, clinical trials of GLP-1 agonists are proceeding in treating or preventing dementia syndrome in patients. If dynamic positron emission tomography (PET) activation to sensory stimuli was able to differentiate patients early on, for example, this type of metabolic approach could be followed by such a biomarker for improvement, lending a personalized approach to therapy.[11] Mediators of neurovascular coupling may also be analyzed for an altered role, such as nitric oxide[22–25] and matrix metallo-proteases.[26] Because the metabolic deficiency is primarily in glucose metabolism, ketone substitution as an alternative brain fuel has been predicted from clinical studies[3] and also applied in animal models of AD.[27] These translational examples highlight how glucose metabolism and neurovascular coupling may be analyzed in a time/age/degeneration profile as well as regional brain assessment and rational interventions developed to improve metabolic supply.

Direct, dynamic recordings of brain glucose and oxygen under a variety of metabolic activation paradigms may reveal the underlying mechanisms of metabolic deficiency in comparison to the degeneration noted as a function of animal age. Both brain glucose and oxygen could be measured with PET dynamic activation as a potential method to highlight patients for specific metabolic interventions.[11] Further, neurovascular coupling to a variety of activation paradigms may be tested in MCI and AD patients to understand the translation of these concepts to the clinical condition.[28] These could be tested with clinical activation including sensory or direct nerve stimulation. Thus, there are numerous translational predictions from these preclinical experiments focused on improving elements of neurovascular coupling and metabolism. For example, metabolic clinical studies (with fluorodeoxyglucose [FDG] PET) comparing efficacy of resting imaging biomarkers to cerebrospinal fluid (CSF) studies[2] show that it is possible to derive additional dynamic biomarkers from maximal increases in blood flow in response to an external stimulus. Further areas within the brain should also be explored with dynamic imaging responses to metabolic challenges, to understand region-specific susceptibility to degeneration, particularly the hippocampus or other critical brain regions. Extension to human analysis of neurovascular coupling will also be critical, as well as studying treatment options focused on mechanisms of neurovascular coupling and rate-limiting steps of glucose uptake and use within the brain.

The next steps in this analysis of underlying pathological mechanisms should include a more detailed understanding of time-related progression of the dementia in relation to neurovascular coupling and substrate supply both in the CVN-AD model as well as in additional, corroborative animal models. Using surrogate markers to estimate neurovascular coupling (in addition to baseline metabolism at rest) may help us understand another dimension of time-related progression from normal aging to MCI.[11] These surrogate markers could be

followed with metabolic treatment in animal models of AD, for example, to see if degeneration could be slowed.[29]

Unlike animal models of AD degeneration, the human progression toward dementia is much less clear and less well defined. Early treatments prior to degeneration can be tested, as in planned studies of earlier, less symptomatic patients.[30–32] However, the earlier the possible prediction of eventual dementia syndrome, the less accurate the prediction. If dementia diagnosis could be more securely established prior to the appearance of severe degeneration, then more aggressive or invasive treatments could be ethically applied at this early time point.[33,34] For example, in Parkinson's disease, response to L-dopa can be used as a surrogate diagnostic test to confirm an early diagnosis, leading to the concept of using early, invasive, deep brain stimulation as a potential disease-modifying treatment compared to optimal medical therapy.[35]

1.2 | Study conclusions

In summary, the significant changes in neurovascular coupling that we report in the CVN-AD model of dementia show both early age onset compared to control animals and involvement of the neocortex, with regional susceptibility of the hippocampus to be more completely evaluated in later studies. These results may be translated using dynamic measurements of neurovascular coupling to provide additional time and region- based biomarkers in predicting early onset of MCI and degeneration in humans. There are several potential avenues of translational, metabolic therapy that could be applied early, such as enhanced glucose transport and ketone availability. Further, depending on the security of early diagnosis, more aggressive, invasive treatments may be tested, in parallel to another degenerative condition, Parkinson's disease.

2 | DETAILED METHODS AND RESULTS

We compared neurovascular coupling in response to K^+ and anoxia in both CVN-AD (APPSwDI +/+ mNOS2 −/−) mice and age-matched C57Bl/6 (WT) mice, to assess metabolic sufficiency and vascular regulation.[19,36,37]

2.1 | *In vivo* mouse preparation

All experiments were approved by the Duke and Durham VA Medical Center Animal Committees and adhered to the National Institutes of Health guide to laboratory animals. Spontaneously breathing mice were anesthetized with isoflurane (≈1.25%) in 30% O_2, then placed in a mouse stereotaxic frame with a nose cone for constant isoflurane inhalation, with a recovery system. The mice were continuously monitored for pulse oxygen saturation (minimum > 90%, average 92.1 ± 3.8%, n = 72 animals, on 30% fiO_2; Mousestat, Kent Scientific), pulse rate (> 400/s; Mousestat, Kent Scientific), and with intermittent tail blood pressure measurements (blood pressure [BP]: > 80 mmHg mean; CODA Monitor, Kent Scientific), using noninvasive recordings, after confirming these non-invasive measurements were concordant with direct arterial recordings of pulse and BP. A total of 72 animals (44 male, 28 female, across three age groups and two genotypes: C57Bl/6 -WT – and CVN-AD) were used: young < 24 weeks; mature 30–40 weeks; aged > 48 weeks. These ages were chosen to be at critical stages of the CVN-AD progression in the neocortex.[18,20]

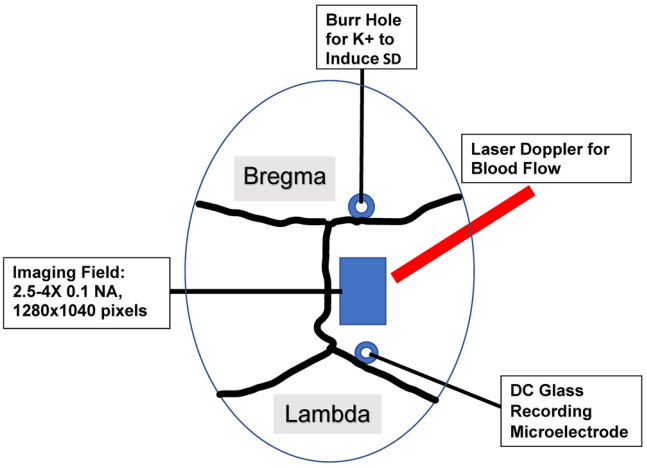

FIGURE 1 *In vivo* mouse setup. The diagram shows the mouse *in vivo* skull format, from above, with burr holes for K^+ anteriorly and the direct current glass recording electrode posteriorly. Blue box shows the imaging field between the burr holes and the red line indicates the laser doppler blood flow probe. The imaging was performed either through a craniotomy (ie, Figure 3) or across the closed mouse skull

After the skull was cleaned of connective tissue and mineral oil applied to increase skull transparency (Figure 1), two 1 mm burr holes were carefully placed: one in front of the coronal suture (for 1 M KCl application) and the second anterior to the lambdoid suture, for placement of a cortical, glass direct current (DC) recording electrode (≈5 MΩ, filled with 0.2 M NaCl). The DC recording electrode used an Ag/AgCl internal wire referenced to an Ag/AgCl ground wire placed into the neck muscles, with the resulting DC extracellular signals amplified (Axon Instruments 1B Multiclamp) and digitized (Digidata 1440 at 1KHz sampling rate). The mice were stabilized for > 30 minutes in the recording setup to assure stability of blood flow and extracellular voltage levels prior to spreading depression (SD) induction. During this period of baseline monitoring, no spontaneous SD events were observed prior to KCl application.

Blood flow was measured by laser doppler (Moore Instruments, 0.46 mm probe) placed on the skull 3.0 mm in front of the microelectrode (located in posterior burr hole). After stabilization for 30 minutes, a small pledget containing 1 M KCl was placed in the anterior burr hole to induce intermittent SD events, which traversed posteriorly to the parietal region; this KCl pledget was left in place for 2 to 3 hours. Previous reports indicated difficulty in inducing SD events with 1.0 M KCl in aged rats (24 months of age), sometimes requiring 3.0 M KCl, vascular occlusion or a KCl crystal.[38,19] However, 1 M KCl

consistently led to SD occurrences in all mouse ages and genotypes.[19] The spread of SD responses across the cortex was also observed using intrinsic optical signaling (IOS) with 562 nm incident light, which is based upon blood flow and blood volume changes, and cell swelling changes.[39–43] IOS reflectance measurements were not only performed transcranially (n = 70 animals) but also confirmed with direct cortical imaging after a craniotomy (n = 2 animals; Figure 3), using oblique light illumination (562 nm, Sutter DG-4). Reflectance from the cortical surface was measured with a Sensicam QE (PCO; 1280 × 1024 pixels, 12-bit pixel depth). The skull was imaged under an upright microscope (2.5–5X, N.A. 0.06–0.12). IOS provides an indirect measure of blood flow and blood volume as the 562 nm illumination is not only strongly absorbed by hemoglobin, but also measures cell swelling.[42] In contrast, laser speckle imaging shows particle movement within blood vessels, similar to the laser doppler.[44] Terminal anoxia was induced with 100% N_2.

2.2 | Image processing

IOS reflectance images of the cortex were taken at 1 Hz frequency (Figure's 1, 3). A control image prior to the traversing SD wave was extracted (Figure 3 top), then subtracted from the 12-bit image stack before and after the SD, calibrated by dividing by the control image, adjusted to ± 10% (ImageJ).[39,42] Values were taken from a 100 × 100 pixel region of interest in the center of the image (Figure 3). The conduction velocity of the wave was calculated directly from the movement of the image wavefront and compared to the physiological conduction velocity, calculated by the delay between the laser doppler probe and the physiological electrode responses.

2.3 | Data analysis

Three different age groups and two genotypes were compared using analysis of variance (ANOVA; if failed testing for normality a nonparametric test was performed). Though animals were of mixed sex, post hoc analysis was also conducted using males only. The specific SD parameters analyzed included conduction velocity, inter-SD time interval, SD voltage amplitude, the percent change of the cerebral blood flow from the baseline (both dip and peak), the area under the blood flow curve (peak amplitude times half-width), and the morphology of the blood flow response (half-width, flow area) and shape, characterized as T1-T6 by Menyhart et al.[19] We also separated the first SD for analysis, because in prior mouse studies this first SD showed an atypical blood flow response, which was followed by a net drop in baseline flow.[16,44,45] Proportional differences in the blood flow responses were analyzed with an X^2 test. For the terminal anoxia the secondary blood flow increase in response to the anoxia was characterized with respect to the baseline (prior to the anoxia) as a percentage (baseline = 100%), the amplitude of the anoxic SD response measured, and the time delay from initiating the N_2 to the anoxic depolarization onset.

3 | RESULTS

3.1 | *In vivo* physiological response to K^+-induced SD

These *in vivo* experiments assessed neurovascular coupling following metabolic activation with K^+-SD, which results in a characteristic, large negative shift of the extracellular potential, reflecting intense neuronal and astrocytic depolarization (Figure 2).[44,46,47] The age groups were selected to span across critical stages of the AD-like histological, vascular, and behavioral progression.[20,29,48,49] Unlike reports across the rat lifespan (i.e., 2 months to 2 years) there was no difference in ease of activation of K^+-SD events across the various mouse ages, which were equally susceptible to the burr hole application of 1 M KCl.[19,38]

Figure 2 shows typical examples of SD waveforms. Note that in both the older WT and CVN-AD animals the SD voltage amplitude showed a trend toward a decrease (Table 1) (not significant - NS). Additionally, the time course and shape of the SD extracellular voltage response were similar across all ages and genotypes.[19] The SD voltage responses also varied within the same animal, depending on the interval from the last SD occurrence and whether there was full propagation across the cortex. Table 1 shows parameters from both the first SD and averaging across all SD occurrences within the same animal.

The time interval between spontaneous SD events did not vary across the ages and genotypes; this interval is a measure of the refractory period before another SD can occur, ranging from 11.5 to 17.6 minutes (Table 1). This time interval is modulated by the anesthesia with slightly fewer SD events occurring in isoflurane compared to other anesthetic agents.[50,51] There were no clusters of SD occurrence. The number of SD occurrences in each animal (over ≈3 hours) also varied from four to seven but was not different between the groups (Table 1). The conduction velocity ranged from 3.8 to 6.9 mm/min but did not significantly vary across age and genotypes (Table 1), whereas in aged rats there was a change in propagation velocity.[38] Thus, the primary difference across ages was the trend toward a reduction in SD amplitude but this was not specific to genotype (Table 1).

In contrast to aging rats (i.e., 24 months) SD events were routinely induced by 1 M KCl applied to the mouse cortex.[19,38] We also consistently observed a trend toward a reduced SD extracellular voltage response in the aged animals, though the analysis of the voltage amplitude of first SD occurrence did not show a significant difference across ages and genotypes (Table 1).[38] The blood flow responses to SD events was primarily hyperemic in these mice, different from the reduced blood flow after the first SD previously reported in young C57Bl/6 mice.[44] The small blood flow dip noted in Figure 4 (in younger mice) suggests small vessel responses to the SD-induced local neuronal depolarization are initiated in the distal capillary bed early during SD, possibly leading to the subsequent reduced blood flow in the larger vessels detected by laser doppler, prior to the initiation of hyperemia.[14] The lack of the dip in the older CVN-AD and aged WT animals suggests reduced, early capillary reactivity, another form of diminished neurovascular coupling, possibly due to extensive

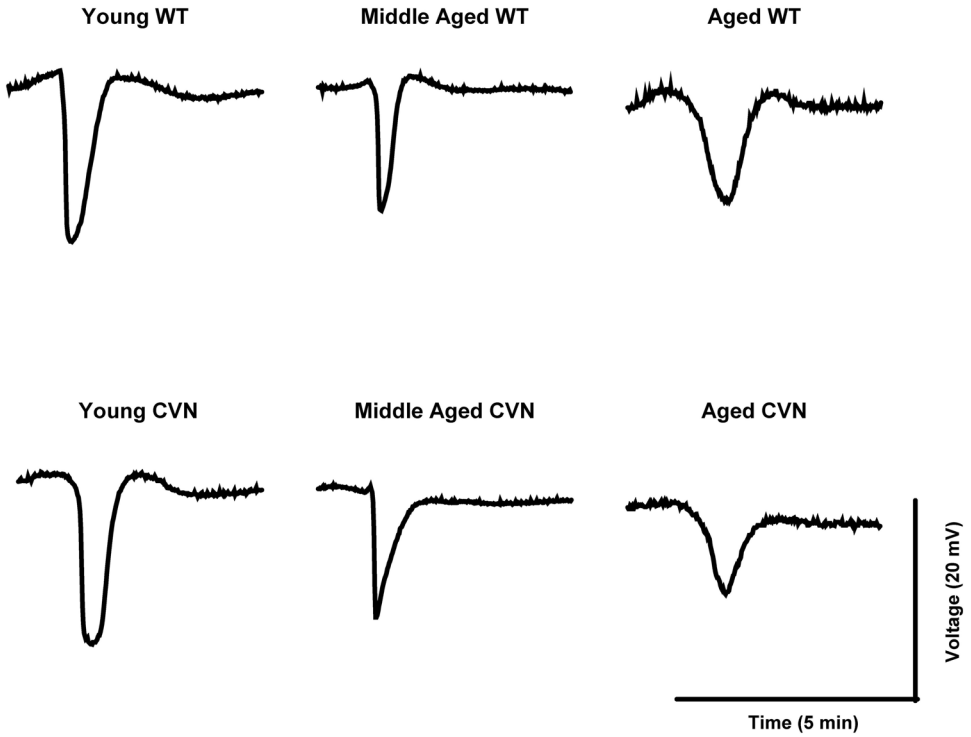

FIGURE 2 Spreading depression voltage waveforms: The amplitude of the young and mid-aged wild-type (WT) and CVN spreading depression (SD) events averaged −11.6 to 16.5 mV whereas the aged WT and CVN animals trended toward smaller SD events (7.7 and 11.6 mV; Table 1), but similar overall waveform shape characteristics. Representative blood flow response and imaging for these SD responses by age and genotype are shown in Figure 4

TABLE 1 Parameters with K^+-SD events

Age	Young	Middle-aged	Aged
# WT /# CVN-AD	(*n* = 7/28) / (*n* = 4/25)	(*n* = 5/36) / (*n* = 6/27)	(*n* = 5/35) / (*n* = 6/38)
First SD occurrence			
SD amplitude (mV)	15.6 ± 7.0 / 16.5 ± 7.0	12.3 ± 7.7 / 11.6 ± 5.	11.6 ± 8.0 / 7.73 ± 5.4
% Change flow peak	177.7 ± 134 / 130.5 ± 179	209.7 ± 112 / 94.3 ± 56	64.0 ± 59.7 / 103.5 ± 54.0*
% Baseline change 1st/2nd SD	90 ± 134 / 12.6 ± 23	41.4 ± 37 / −4.4 ± 10.4	−46.4 ± 48.4 / −23.1 ± 53.2*
All SD occurrences averaged per mouse			
% Change flow peak	98.2 ± 10.9 / 103.2 ± 66.2	100.9 ± 47.6 / 92.7 ± 46.6	101.6 ± 52.4 / 67.3 ± 45.2*
% Change flow dip	−43.8 ± 10.9 / −20.6 ± 18.8	−34.4 ± 21.1 / −16.4 ± 12.7	−13.2 ± 29.4 / −11.9 ± 20.0**
Flow halfwidth (sec)	232 ± 183 / 314 ± 180	240 ± 160 / 159 ± 98	143 ± 107** / 137 ± 98**
Flow area (%*min/100)	4.42 ± 4.2 / 5.3 ± 2.0	4.42± 2.4 / 2.92 ± 1.63	2.24 ± 1.2 / 1.59 ± 0.56**
Time between SDs (min)	14.0 ± 9.64 / 17.6 ± 4.2	16.9 ± 3.2 / 17.6 ± 5.31	11.5 ± 2.4 / 16.6 ± 6.48
Total # SD events/mouse	4.0 ± 1.4 / 6.3 ± 2.3	7.2 ± 2.8 / 4.5 ± 2.8	7.0 ± 1.58 / 6.14 ± 3.63
SD velocity (mm/min)	6.66 ± 2.25 / 5.2 ± 1.6	3.84 ± 1.5 / 4.25 ± 3.6	6.85 ± 6.28 / 4.62 ± 1.53

Notes: Data are shown as mean ± standard deviation comparing the WT and CVN animals at the same age (# animals/# events across animals). The net flow change above and below baseline is expressed as a % of the baseline value (because the baseline flow values are variable and cannot be calibrated). Asterisks denote significance: $P \leq 0.01$ is *, 0.001 is **, versus the age-matched control with ANOVA.
Abbreviations: ANOVA, analysis of variance; SD, spreading depression; WT, wild type.

capillary amyloid angiopathy in this model.[16,48,52] It is also important to point out that the isoflurane anesthesia may also affect the number of SD occurrences but does not affect other parameters of SD cerebral blood flow (CBF) responses on detailed comparisons with other anesthetics.[45,51,53] Mice under spontaneous respirations with isoflurane may show a lower pCO_2 (ie, ≈27 mmHg)[54] than those undergoing intubation/tracheostomy, paralysis, and mechanical ventilation (i.e., ≈40–44 mmHg).[16,44,45] However, the mice in this study with

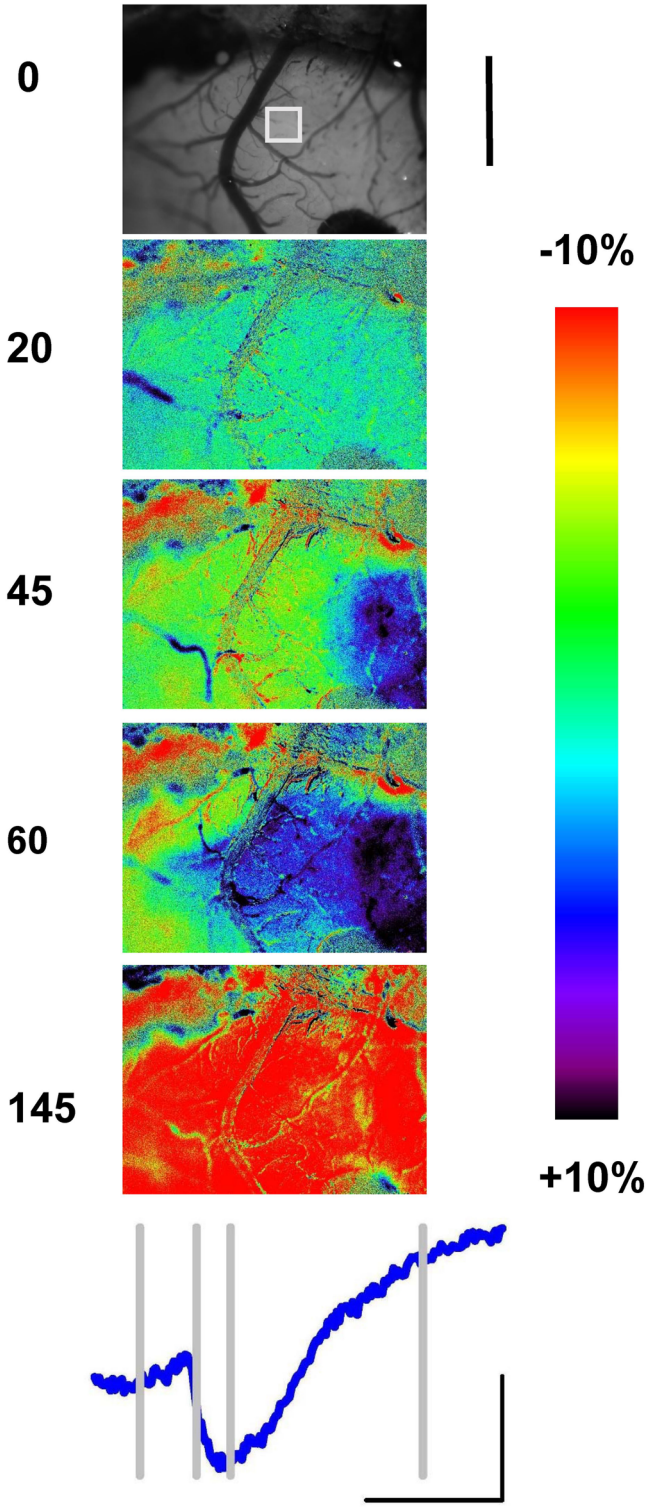

FIGURE 3 K^+-spreading depression (SD) imaging: The upper image is a direct view of the right mouse brain through a craniotomy (from an 8-week-old control C57Bl mouse), illuminated at 562 nm, with reflectance from an oblique light source detected by a Sensicam QE camera. The boundaries are midline on the upper side, anterior to the right, and posterior to the left (as in Figure 1). Below are inverted difference images (subtracted from the control image [top] and normalized by the control, ± 10%) at intervals (sec) during the spreading depression advance across the cortex (from right, anterior to left, posterior). The reflectance shows increased reflectance with decreased blood flow and blood volume, hence the scale is inverted to correspond to blood flow rather than reflectance. This allows better correlation with Figure 4 and a direct correlation to blood flow and blood volume. At the bottom is a region of interest plot from the center of the images with the timing of each progressive image shown as vertical bars. There is initially a background green (at 20 seconds) representing no difference, then a brighter green advancing wavefront at the onset of the spreading depression (at 45 seconds), showing the time of increased blood flow just before the dip occurs. Note at 45 seconds, there is a small blue region to the right, whereas at 60 seconds, the blue region (representing increased reflectance) has advanced to the center of the image. The blue area corresponds to decreased blood flow and represents the advancing dip. At 175 seconds the entire image shows decreased reflectance but increased blood flow (red). The vertical calibration line shows 1.0 mm distance. The bottom graph shows 1 min horizontally and 10% difference vertically

spontaneous breathing maintained normal physiological parameters for at least 3 to 4 hours (i.e., pulse oxygenation, blood pressure) indicating that, regardless of pCO_2, the conditions were physiologically appropriate. This large difference in respiratory parameters may partially result in the different first SD response noted here, because no SD events were noted prior to the first SD after KCl application.

3.2 | Cortical IOS imaging of K^+-SD events

Figure 3 shows the typical light reflectance imaging (IOS) spread of the SD across the exposed cortex, from anterior (right) to posterior (left), highlighted on the graph below with the gray bars indicating the specific imaging time points.[39,41,55] The reflectance becomes negative with less light return, indicating increased absorbance by the tissue and hemoglobin; hence we have inverted the scale to correspond closely to the blood flow (i.e., red represents increased blood flow, blue represents decreased blood flow). The green image at 20 seconds indicates no difference, whereas there is a reflectance decrease at 45 seconds (brighter green; blood flow increase). The SD wave then shows a blue region (with increased reflectance and decreased blood flow) at 60 seconds as the SD wave progresses across the cortex, corresponding to a blood flow dip. Then, there is a prolonged red area by 145 seconds (decreased reflectance; increased blood flow). The bottom graph shows the inverted IOS results (from the region of interest) plotted out over time (as in Figure 4, where the IOS is superimposed with blood flow responses). The imaging was also performed across the mouse skull with the same result, showing the SD wavefront phases and subsequent recovery.[40,41] SD propagation conduction velocity from the IOS averaged ≈6 mm/min and did not vary by age or genotype (Table 1). These results show that the K^+-SD event can be tracked across the cortex to verify conduction toward the recording electrode, and the reflectance measurements can be directly correlated with the blood flow responses (Figure 4) for each IOS component (i.e., blood flow, blood volume, and cell swelling).

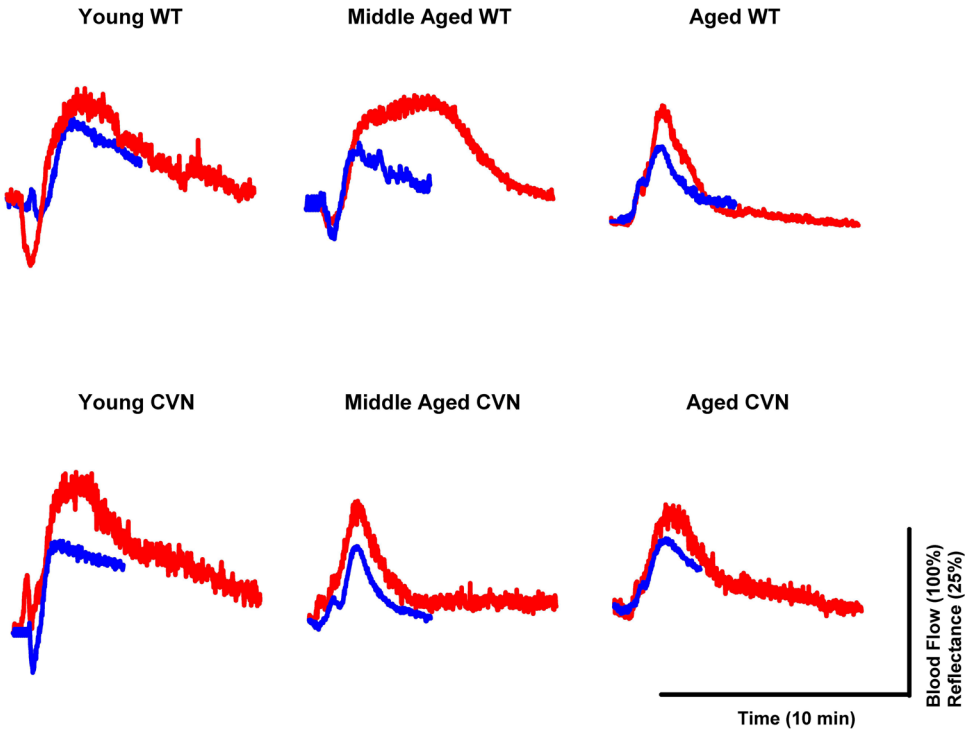

FIGURE 4 K^+-spreading depression (SD) blood flow and imaging signals: These representative examples of the blood flow response (red) to typical spreading depression episodes (as in Figure 2) are shown for each age and genotype group. The net increased flow above the baseline was normalized by the baseline value to show % values above baseline, and decreased flow during the dip also normalized to % (Table 1). The absolute baseline values for each representative example were (in arbitrary flux units): Young WT 95, Young CVN 92, Middle Aged WT 106, Middle Aged CVN 56, Aged WT 87, and Aged CVN 120. An average region of interest from the center of the imaging field (100 × 100 pixels, as in Figure 3) was measured across the spreading depression images, with an increased imaging signal (IOS; blue) representing a decreased reflectance from the cortex (using an oblique 562 nm light source). The reflectance images are inverted (as in Figure 3) to correspond directly to the blood flow amplitude, and also are % referenced to the baseline values. The imaging was only typically carried out to 5 minutes so the IOS responses are shorter than the cerebral blood flow data. These responses were similar whether imaged through an open craniotomy (ie, Figure 3) or across the closed skull (not shown). The blood flow response (red traces) reliably showed an increased blood flow for both the first and subsequent SD events in all animals, but in many cases after an initial decrease or dip. Note that during the blood flow dip (if present) there is an increased imaging reflectance, then a decrease during the blood flow overshoot, indicating the strong hemoglobin absorbance of the 562 nm light. Average shape values are given in Table 1 for each group and the shape characteristics defined further in Figure 5, including the amplitude of the dip.[19] The young WT, young CVN, and middle-aged WT all show a pronounced early dip, corresponding to T3 phenotype, whereas the young CVN demonstrates a more moderate dip (T4). The remainder are T2 without a dip. Overall, the middle-aged CVN and both aged groups showed less dip and a simpler monotonic, shorter duration blood flow response. The amplitude and duration of the blood flow response are shown in Table 1 along with net area

Intrinsic optical signals measured across the skull have proven consistently useful to monitor SD spread across the neocortex[40,41] and in brain slices.[39,42] Changes in cell swelling are insensitive to illumination frequency,[42] and are particularly pronounced with SD events, reflecting the severe ion and water movement as cells depolarize and then repolarize. The small discrepancy between the blood flow and IOS responses (noted in Figure 4) show this second, swelling component of the IOS reflectance, in addition to the blood flow and volume from hemoglobin absorption.

3.3 | SD-induced blood flow and correlative IOS imaging

A robust, hyperemic blood flow response occurred across all SD events, ages, and genotypes (Table 1), similar to aged rats with no AD pathology.[19,38] Figure 4 shows typical, individual CBF responses (red) and simultaneous IOS imaging time sequences (blue, similar to Figure 3). Note that all events demonstrated a positive blood flow, though young mice also showed a dip prior to the increase; this prelude dip became less common with age and CVN-AD progression (Table 1). As in Figure 3 the blood flow and inverted IOS signals were parallel in terms of the initial blood flow dip, showing an increased IOS reflectance during the dip (i.e., blue regions in Figure 3, as noted in Figure 4 young and middle- aged WT). As the blood flow increased there was a large decrease in the IOS reflectance (red region in Figure 3) because hemoglobin strongly absorbs the 562 nm light, hence reducing light return to the detector.[55] The other three examples (i.e., WT aged and CVN middle-aged and aged) show neither an initial blood flow dip nor a drop in the IOS response below baseline, demonstrating the tight correlation between the two events. However, as in brain slices,[39,42] there is also a tissue swelling response within cells, detected

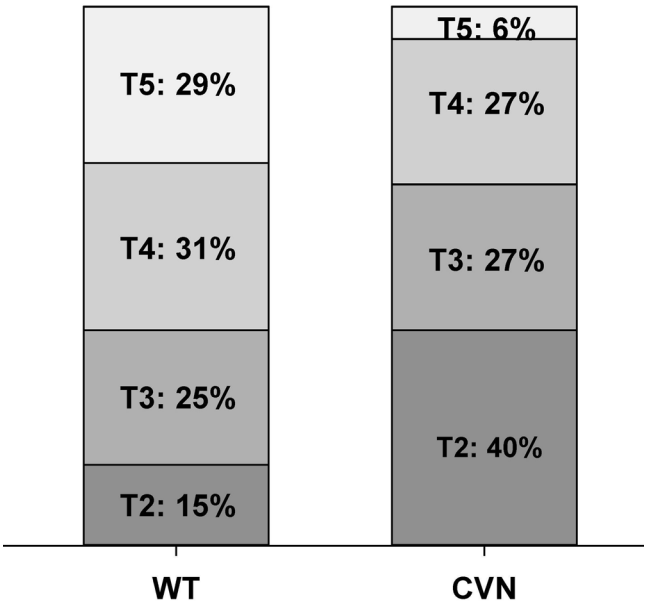

FIGURE 5 Blood flow shapes: The blood flow shapes are characterized as T1–T6 in rats, but also are applicable in mice,[19] with T1–T4 showing a mainly positive blood flow response with or without an initial dip; T5 and T6 are predominantly a negative blood flow response. The bar chart shows the T2–T5 types categorized between WT and CVN-AD (neither T1 nor T6 shapes were observed). The relative percent of each blood flow morphology is shown within each box. Across the wild type (WT) ages there was no overall difference in shape characteristics, and likewise across the CVN age groups there was no difference. However, there was a significant difference ($P < 0.001$; Chi-square tests for proportions) across all groups (i.e., WT + CVN) and also for each age group between the WT and CVN

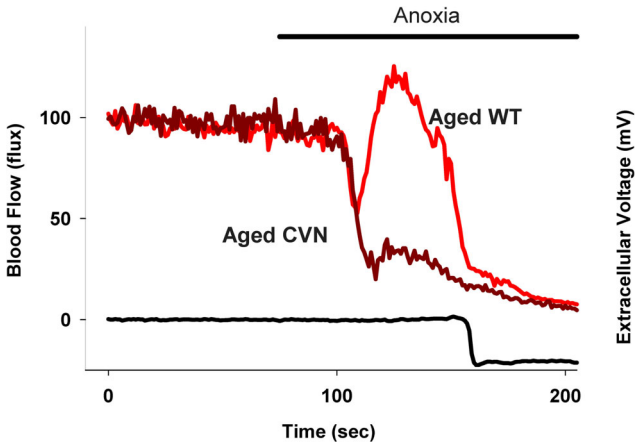

FIGURE 6 Anoxia-induced blood flow rebound: The reaction to anoxia includes a sharp decrease in cerebral blood flow, a secondary blood flow rebound representing cerebral autoregulation in the face of declining system blood pressure, then a slow decline to zero cerebral blood flow as systemic blood flow wanes. The anoxic spreading depression (physiological trace in black) typically appears just after the rebound falls to near baseline, which is shown below the blood flow responses as the voltage suddenly drops. The rebound is shown as the secondary peak in this representative example, which is significantly enhanced in the wild-type aged animals (bright red trace), in comparison to the CVN aged animals (dark red trace). Values are in Table 2. The physiology scale is the same as on the left for blood flow

indirectly as an asymmetry between the blood flow and IOS (i.e., the two responses are parallel but not identical, confirming both blood flow and swelling elements in the IOS).

The blood flow changes above (peak) and below (dip) baseline (Table 1) were analyzed for the first SD alone, individually, and also after averaging within the same animal (Table 1). Analyzing across either the first SD or all SD occurrences there was a significant effect of age in both the WT and the CVN group (by ANOVA, $P = 0.009$), primarily between the aged WT and CVN groups, with a reduction in peak amplitude of the blood flow hyperemic response in the CVN-AD aged compared to WT aged animals for the entirety of the SD occurrences (but paradoxically not for the first SD, likely due to the small sample sizes). When male mice were analyzed separately in the young and aged groups the differences were similar, indicating these CVN-AD reductions in peak blood flow response were not sex specific. Likewise, there was a significant decrease in dip amplitude as a function of age and CVN status (Table 1), corresponding to the reduced dip noted in Figure 4. In previous reports of mouse SD the first SD was anomalous, with reduced blood flow and a drop in the baseline.[16,44,45] In contrast, we observed a rise of the baseline blood flow values between the first and second SD in the young and middle-aged groups, but a decrease in aged wild type and CVN animals (Table 1).

As also noted in Figure 4 the young WT and CVN-AD animals demonstrated a prolonged SD-induced blood flow hyperemic response (measured as flow halfwidth and flow area). However, the duration of the CBF response decreased significantly with age in WT and both middle-aged and aged CVN-AD mice (by ANOVA: $P \leq 0.001$; Table 1). To assess global hyperemia, we also measured the area under the curve of the blood flow response (i.e., peak blood flow times the halfwidth). This was significantly different only across the CVN-AD animals ($P = 0.001$), showing a decreased blood flow response with age (Table 1). Overall, there was a significant but premature reduction in the CVN-AD middle-aged and aged animals compared to the WT age-matched controls in blood flow response to the SD events, indicating an earlier deficiency in CVN-AD neurovascular coupling.

3.4 | SD blood flow waveform shapes

Shapes of SD hyperemic blood flow in response to SD occurrences were characterized into positive responses (i.e., T2; Figure 4), those with an initial dip (i.e., T1, T3, and T4), and negative responses (i.e., T5, T6).[19] Though these responses were characterized in rats the separation may also be helpful in describing these mouse SD events. Figure 5 shows a bar graph of the various waveform shapes plotted as WT versus CVN as there was no difference within each genotype, with almost all in the T2–T5 category (i.e., T1 and T6 rare). Note the shift between the two genotypes,[19] which on X^2 testing of proportions showed a significant difference between the WT and CVN-AD responses ($P = 0.001$), whereas there was no difference noted between either the WT across age alone or the CVN-AD across age alone. This graph confirms the simpler, monotonic blood flow response occurs earlier in the CVN-AD mice compared to the WT, as shown in Figure 4.

TABLE 2 Parameters with anoxia and anoxic depolarization events

Age	Young	Middle-aged	Aged
# WT / # CVN-AD	7 / 4	5 / 6	5 / 6
Ratio flow rebound (%)	114 ± 42 / 71 ± 22	85 ± 12 / 131 ± 60	141 ± 75 / 54 ± 27**
Anoxic SD amplitude (mV)	13.3 ± 5.98 / 13.0 ± 9.2	13.8 ± 7.92 / 13.6 ± 6.72	17.0 ± 6.72 / 14.2 ± 7.62
N_2 to anoxic SD (min)	3.24 ± 3.91 / 2.06 ± 0.51	1.42 ± 1.49 / 1.84 ± 1.2	1.64 ± 0.59 / 1.11 ± 0.67

Notes: Data are shown as mean ± standard deviation (# animals). The flow rebound is a ratio to the baseline flow values (100%). Asterisks denote significant differences with $P = 0.01$ * and $P = 0.001$ **.
Abbreviations: SD, spreading depression; WT, wild type.

3.5 | Anoxia responses

After anoxia was introduced (100% N_2) there was initially a sharp drop in blood flow (Figure 6).[56] However, within 10 to 20 seconds there was a compensatory rebound increase in blood flow in most animals, before terminal blood flow collapse occurred (Figure 6) and a subsequent anoxic depolarization (Table 2). Figure 6 also shows when the anoxic spreading depression occurs (lower trace), typically after the rebound increase in CBF has waned. Aged CVN-AD mice demonstrated a significant reduction of the reactive blood flow magnitude during this initial phase of the anoxic response, compared to both the middle-aged ($P = 0.025$) CVN-AD as well as the aged WT mice ($P = 0.02$; Table 2). However, there was no difference in the anoxic depolarization amplitude or the delay from the onset of N_2 to the occurrence of the anoxic depolarization (Table 2), across ages and genotypes. These findings indicate significantly less autoregulation and resilience in response to this severe, pathological metabolic challenge, particularly in the aged CVN group, another form of dampened regulatory vascular coupling.

ACKNOWLEDGMENTS

These studied were supported by NIH R21 AG051103 (DAT), VA I21 RX002223 (DAT), and VA I21 BX003023 (DAT).

CONFLICTS OF INTEREST

The authors have no conflicts of interest to declare.

REFERENCES

1. Hachinski V, Einhäupl K, Ganten D, et al. Preventing dementia by preventing stroke: the Berlin Manifesto. *Alzheimer's & Dementia: The Journal of the Alzheimer's Association*. 2019;15(7):961-984.
2. Caminiti SP, Ballarini T, Sala A, et al. FDG-PET and CSF biomarker accuracy in prediction of conversion to different dementias in a large multicentre MCI cohort. *NeuroImage Clinical*. 2018;18:167-177.
3. Croteau E, Castellano CA, Fortier M, et al. A cross-sectional comparison of brain glucose and ketone metabolism in cognitively healthy older adults, mild cognitive impairment and early Alzheimer's disease. *Exp Gerontol*. 2018;107:18-26.(doi): phttps://doi.org/10.1016/j.exger.2017.1007.1004. Epub 2017 Jul 1012.
4. Cai W, Zhang K, Li P, et al. Dysfunction of the neurovascular unit in ischemic stroke and neurodegenerative diseases: an aging effect. *Ageing Res Rev*. 2017;34:77-87.(doi): phttps://doi.org/10.1016/j.arr.2016.1009.1006. Epub 2016 Sep 1030.
5. Sweeney MD, Montagne A, Sagare AP, et al. Vascular dysfunction-The disregarded partner of Alzheimer's disease. *Alzheimers Dement*. 2019;15(1):158-167.
6. Winkler EA, Nishida Y, Sagare AP, et al. GLUT1 reductions exacerbate Alzheimer's disease vasculo-neuronal dysfunction and degeneration. *Nat Neurosci*. 2015;18(4):521-530. doi: 510.1038/nn.3966. Epub 2015 Mar 1032.
7. Kisler K, Nelson AR, Montagne A, et al. Cerebral blood flow regulation and neurovascular dysfunction in Alzheimer disease. *Nat Rev Neurosci*. 2017;18(7):419-434. doi: 410.1038/nrn.2017.1048. Epub 2017 May 1018.
8. Gibas KJ. The starving brain: overfed meets undernourished in the pathology of mild cognitive impairment (MCI) and Alzheimer's disease (AD). *Neurochem Int*. 2017;110:57-68.(doi): phttps://doi.org/10.1016/j.neuint.2017.1009.1004. Epub 2017 Sep 1019.
9. An Y, Varma VR, Varma S, et al. Evidence for brain glucose dysregulation in Alzheimer's disease. *Alzheimers Dement*. 2018;14(3):318-329. doi: 310.1016/j.jalz.2017.1009.1011. Epub 2017 Oct 1019.
10. Blonz ER. Alzheimer's Disease as the Product of a Progressive Energy Deficiency Syndrome in the Central Nervous System: the Neuroenergetic Hypothesis. *Journal of Alzheimer's Disease: JAD*. 2017;60(4):1223-1229. doi: 1210.3233/JAD-170549.
11. Chiaravalloti A, Micarelli A, Ricci M, et al. Evaluation of Task-Related Brain Activity: is There a Role for (18)F FDG-PET Imaging?. *Biomed Res Int*. 2019;2019:4762404.
12. Alzheimer's Association Calcium Hypothesis Workgroup. Calcium hypothesis of Alzheimer's disease and brain aging: a framework for integrating new evidence into a comprehensive theory of pathogenesis. *Alzheimer's & Dementia : The Journal of the Alzheimer's Association* 2017;13(2):178-182.e117.
13. Turner DA. Neurovascular regulation is critical for metabolic recovery from spreading depression. *Brain*. 2014;137(Pt 11):2877-2878. doi: 2810.1093/brain/awu2263. Epub 2014 Oct 2824.
14. Ayata C, Lauritzen M. Spreading Depression, Spreading Depolarizations, and the Cerebral Vasculature. *Physiol Rev*. 2015;95(3):953-993.
15. Kim J, Jeong Y. Augmentation of sensory-evoked hemodynamic response in an early Alzheimer's disease mouse model. *Journal of Alzheimer's Disease : JAD*. 2013;37(4):857-868.
16. Shin HK, Jones PB, Garcia-Alloza M, et al. Age-dependent cerebrovascular dysfunction in a transgenic mouse model of cerebral amyloid angiopathy. *Brain*. 2007;130(Pt 9):2310-2319. doi: 2310.1093/brain/awm2156. Epub 2007 Jul 2316.
17. Hartings JA, Shuttleworth CW, Kirov SA, et al. The continuum of spreading depolarizations in acute cortical lesion development: examining Leao's legacy. *J Cereb Blood Flow Metab*. 2017;37(5):1571-1594. doi: 1510.1177/0271678×16654495. Epub 16652016 Jan 16654491.
18. Colton CA, Wilson JG, Everhart A, et al. mNos2 deletion and human NOS2 replacement in Alzheimer disease models. *J Neuropathol Exp Neurol*. 2014;73(8):752-769.
19. Menyhart A, Makra P, Szepes BE, et al. High incidence of adverse cerebral blood flow responses to spreading depolarization in the aged ischemic rat brain. *Neurobiol Aging*. 2015;36(12):3269-3277. doi: 3210.1016/j.neurobiolaging.2015.3208.3014. Epub 2015 Aug 3218.

20. Wilcock DM, Lewis MR, Van Nostrand WE, et al. Progression of amyloid pathology to Alzheimer's disease pathology in an amyloid precursor protein transgenic mouse model by removal of nitric oxide synthase 2. *The Journal of Neuroscience : The Official Journal of the Society for Neuroscience*. 2008;28(7):1537-1545.
21. Gejl M, Brock B, Egefjord L, et al. Blood-Brain Glucose Transfer in Alzheimer's disease: effect of GLP-1 Analog Treatment. *Sci Rep*. 2017;7(1):17490. doi: 17410.11038/s41598-17017-17718-y.
22. Dias C, Lourenco CF, Ferreiro E, et al. Age-dependent changes in the glutamate-nitric oxide pathway in the hippocampus of the triple transgenic model of Alzheimer's disease: implications for neurometabolic regulation. *Neurobiol Aging*. 2016;46:84-95.(doi): phttps://doi.org/10.1016/j.neurobiolaging.2016.1006.1012. Epub 2016 Jun 1029.
23. Hosford PS, Gourine AV. What is the key mediator of the neurovascular coupling response?. *Neurosci Biobehav Rev*. 2019;96:174-181.(doi): phttps://doi.org/10.1016/j.neubiorev.2018.1011.1011. Epub 2018 Nov 1024.
24. Lourenco CF, Ledo A, Caetano M, et al. Age-Dependent Impairment of Neurovascular and Neurometabolic Coupling in the Hippocampus. *Front Physiol*. 2018;9:913. (doi): phttps://doi.org/10.3389/fphys.2018.00913. eCollection 02018.
25. Nippert AR, Biesecker KR, Newman EA. Mechanisms Mediating Functional Hyperemia in the Brain. *Neuroscientist*. 2018;24(1):73-83. https://doi.org/10.1177/1073858417703033. Epub 1073858417702017 Apr 1073858417703012.
26. Ridnour LA, Dhanapal S, Hoos M, et al. Nitric oxide-mediated regulation of beta-amyloid clearance via alterations of MMP-9/TIMP-1. *J Neurochem*. 2012;123(5):736-749.
27. Zilberter M, Ivanov A, Ziyatdinova S, et al. Dietary energy substrates reverse early neuronal hyperactivity in a mouse model of Alzheimer's disease. *J Neurochem*. 2013;125(1):157-171.
28. Levit A, Hachinski V, Whitehead SN. Neurovascular unit dysregulation, white matter disease, and executive dysfunction: the shared triad of vascular cognitive impairment and Alzheimer disease. *Geroscience*. 2020;42(2):445-465.
29. Kan MJ, Lee JE, Wilson JG, et al. Arginine deprivation and immune suppression in a mouse model of Alzheimer's disease. *J Neurosci*. 2015;35(15):5969-5982. doi: 5910.1523/JNEUROSCI.4668-5914.2015.
30. Naro A, Corallo F, De Salvo S, et al. Promising Role of Neuromodulation in Predicting the Progression of Mild Cognitive Impairment to Dementia. *J Alzheimers Dis*. 2016;53(4):1375-1388. doi: 1310.3233/JAD-160305.
31. Sur S, Lin Z, Li Y, et al. Association of cerebrovascular reactivity and Alzheimer pathologic markers with cognitive performance. *Neurology*. 2020;95(8):e962-e972.
32. Vecchio F, Miraglia F, Iberite F, et al. Sustainable method for Alzheimer dementia prediction in mild cognitive impairment: electroencephalographic connectivity and graph theory combined with apolipoprotein E. *Ann Neurol*. 2018;84(2):302-314. doi: 310.1002/ana.25289. Epub 22018 Aug 25225.
33. Chang CH, Lane HY, Lin CH. Brain Stimulation in Alzheimer's Disease. *Front Psychiatry*. 2018;9:201. (doi): phttps://doi.org/10.3389/fpsyt.2018.00201. eCollection 02018.
34. Lozano AM, Fosdick L, Chakravarty MM, et al. A Phase II Study of Fornix Deep Brain Stimulation in Mild Alzheimer's Disease. *J Alzheimers Dis*. 2016;54(2):777-787. doi: 710.3233/JAD-160017.
35. Hacker ML, Turchan M, Heusinkveld LE, et al. Deep brain stimulation in early-stage Parkinson disease: five-year outcomes. *Neurology*. 2020;95(4):e393-e401.
36. Galeffi F, Somjen GG, Foster KA, et al. Simultaneous monitoring of tissue PO2 and NADH fluorescence during synaptic stimulation and spreading depression reveals a transient dissociation between oxygen utilization and mitochondrial redox state in rat hippocampal slices. *J Cereb Blood Flow Metab*. 2011;31(2):626-639.
37. Menyhart A, Zolei-Szenasi D, Puskas T, et al. Age or ischemia uncouples the blood flow response, tissue acidosis, and direct current potential signature of spreading depolarization in the rat brain. *Am J Physiol Heart Circ Physiol*. 2017;313(2):H328-H337. doi: 310.1152/ajpheart.00222.02017. Epub 02017 Jun 00229.
38. Guedes RCA, Abadie-Guedes R. Brain Aging and Electrophysiological Signaling: revisiting the Spreading Depression Model. *Front Aging Neurosci*. 2019;11:136. (doi): phttps://doi.org/10.3389/fnagi.2019.00136. eCollection 02019.
39. Aitken PG, Tombaugh GC, Turner DA, et al. Similar propagation of SD and hypoxic SD-like depolarization in rat hippocampus recorded optically and electrically. *J Neurophysiol*. 1998;80(3):1514-1521. doi: 1510.1152/jn.1998.1580.1513.1514.
40. Chen S, Feng Z, Li P, et al. In vivo optical reflectance imaging of spreading depression waves in rat brain with and without focal cerebral ischemia. *J Biomed Opt*. 2006;11(3):34002. doi: 34010.31117/34001.2203654.
41. Chung DY, Sugimoto K, Fischer P, et al. Real-time non-invasive in vivo visible light detection of cortical spreading depolarizations in mice. *J Neurosci Methods*. 2018;309:143-146.(doi): phttps://doi.org/10.1016/j.jneumeth.2018.1009.1001. Epub 2018 Sep 1015.
42. Fayuk D, Aitken PG, Somjen GG, et al. Two different mechanisms underlie reversible, intrinsic optical signals in rat hippocampal slices. *J Neurophysiol*. 2002;87(4):1924-1937. doi: 1910.1152/jn.00231.02001.
43. Foster KA, Beaver CJ, Turner DA. Interaction between tissue oxygen tension and NADH imaging during synaptic stimulation and hypoxia in rat hippocampal slices. *Neuroscience*. 2005;132(3):645-657.
44. Yuzawa I, Sakadzic S, Srinivasan VJ, et al. Cortical spreading depression impairs oxygen delivery and metabolism in mice. *J Cereb Blood Flow Metab*. 2012;32(2):376-386. doi: 310.1038/jcbfm.2011.1148. Epub 2011 Oct 1019.
45. Ayata C, Dunn AK, Gursoy OY, et al. Laser speckle flowmetry for the study of cerebrovascular physiology in normal and ischemic mouse cortex. *J Cereb Blood Flow Metab*. 2004;24(7):744-755.
46. Fordsmann JC, Ko RW, Choi HB, et al. Increased 20-HETE synthesis explains reduced cerebral blood flow but not impaired neurovascular coupling after cortical spreading depression in rat cerebral cortex. *J Neurosci*. 2013;33(6):2562-2570. doi: 2510.1523/JNEUROSCI.2308-2512.2013.
47. Piilgaard H, Lauritzen M. Persistent increase in oxygen consumption and impaired neurovascular coupling after spreading depression in rat neocortex. *J Cereb Blood Flow Metab*. 2009;29(9):1517-1527. doi: 1510.1038/jcbfm.2009.1573. Epub 2009 Jun 1510.
48. Van Nostrand WE, Xu F, Rozemuller AJ, et al. Enhanced capillary amyloid angiopathy-associated pathology in Tg-SwDI mice with deleted nitric oxide synthase 2. *Stroke*. 2010;41(10 Suppl):S135-S138.
49. Wilcock DM, Vitek MP, Colton CA. Vascular amyloid alters astrocytic water and potassium channels in mouse models and humans with Alzheimer's disease. *Neuroscience*. 2009;159(3):1055-1069.
50. Kudo C, Nozari A, Moskowitz MA, et al. The impact of anesthetics and hyperoxia on cortical spreading depression. *Exp Neurol*. 2008;212(1):201-206.
51. Kudo C, Toyama M, Boku A, et al. Anesthetic effects on susceptibility to cortical spreading depression. *Neuropharmacology*. 2013;67:32-36.
52. Park L, Koizumi K, Jamal SEI, et al. Age-dependent neurovascular dysfunction and damage in a mouse model of cerebral amyloid angiopathy. *Stroke*. 2014;45(6):1815-1821. doi: 1810.1161/STROKEAHA.1114.005179. Epub 002014 Apr 005129.
53. Tsurugizawa T, Takahashi Y, Kato F. Distinct effects of isoflurane on basal BOLD signals in tissue/vascular microstructures in rats. *Sci Rep*. 2016;6:38977.

54. Wang Z, Schuler B, Vogel O, et al. What is the optimal anesthetic protocol for measurements of cerebral autoregulation in spontaneously breathing mice?. *Exp Brain Res*. 2010;207(3-4):249-258.
55. Chen S, Li P, Luo W, et al. Time-varying spreading depression waves in rat cortex revealed by optical intrinsic signal imaging. *Neurosci Lett*. 2006;396(2):132-136. doi: 110.1016/j.neulet.2005.1011.1025. Epub 2005 Dec 1013.
56. Shin HK, Dunn AK, Jones PB, et al. Vasoconstrictive neurovascular coupling during focal ischemic depolarizations. *J Cereb Blood Flow Metab*. 2006;26(8):1018-1030. doi: 1010.1038/sj.jcbfm.9600252. Epub 9602005 Dec 9600257.

How to cite this article: Turner DA, Degan S, Hoffmann U, Galeffi F, Colton CA. CVN-AD Alzheimer's mice show premature reduction in neurovascular coupling in response to spreading depression and anoxia compared to aged controls. *Alzheimer's Dement*. 2021;17:1109–1120.
https://doi.org/10.1002/alz.12289